Construction of Ti_3C_2/BiOBr heterojunction for efficient removal of antibiotics

Y. Zhong[a], K. Lei[a], Y. J. Duan[a], X. H. Zeng[a], L. J. Mao[a], S. J. Hu[a], H. R. Dong[a], S. M. Lv[a], R. Xiong[b], Y. Sun[a,*]

[a]*School of Mechanical Engineering, Chengdu University, Chengdu, 610106, China*

[b]*School of Architecture and Civil Engineering, Chengdu University, Chengdu, 610106, China*

Layered Ti_3C_2 was prepared by etching Ti_3AlC_2 powder with hydrofluoric acid, and Ti_3C_2/BiOBr (TB) composites was successfully synthesized via in-situ deposition method. The effects of BiOBr content in the composites on their crystal structure, morphology and photocatalytic properties were systematically discussed. The experimental results indicate that the Ti_3C_2 introduction can promote the degradation of tetracycline owing to fast separation of photoexcited charge carriers. When the mass ratios of Ti_3C_2 to BiOBr were 1:50, Ti_3C_2/BiOBr exhibited the highest removal efficiency of 80.3% after 30 min of illumination. Furthermore, a possible degradation mechanism was clarified by the band structure and the trapping experiment.

(Received June 24, 2024; Accepted September 10, 2024)

Keywords: Ti_3C_2/BiOBr, Composite materials, Heterojunction, Photocatalytic degradation

1. Introduction

Tetracycline (TC) is an extensively used antimicrobial, which has an inhibitory effect on most negative bacteria. However, the overuse of antibiotics has a certain harm to the environment and human health. At present, common methods such as adsorption, biodegradation and photocatalysis have been developed to degrade antibiotics [1-3]. Among them, photocatalysis technology can be regarded as an effective wastewater treatment method [4-6]. BiOBr is an excellent photocatalyst with high chemical stability and suitable bandgap energy, but the rapid combination rate of photogenerated carriers limits its application [7-9]. Thus, enhancing the photocatalytic performance of pure BiOBr through heterojunction construction proves to be an effective strategy. Transition metal carbides (MXenes), new two-dimensional materials with large specific surface area, surface end group and good electrical conductivity, have been widely applied in environmental treatment, clean energy, and sensors [10-12]. Ti_3C_2 Mxene, a new 2D layered material [13-15], has great potential to couple with BiOBr hybrid catalyst to achieve superior photocatalytic performance.

In this study, multilayer Ti_3C_2 was prepared by etching of Ti_3AlC_2 powder and BiOBr microspheres were in-situ grown on the Ti_3C_2 surface by deposition to produce a heterojunction

* Corresponding author: sunyan@cdu.edu.cn

https://doi.org/10.15251/DJNB.2024.193.1301

structure. The study discussed the impact of the mass ratios of Ti_3C_2 to BiOBr on the structure and morphology and photocatalytic degradation. Additionally, we proposed a potential mechanism of the improved photocatalytic activity observed in Ti_3C_2/BiOBr.

2. Experimental

2.1. Preparation

Ti_3C_2 was prepared according to previous literature [16]. First, 0.5 g of Ti_3AlC_2 was added to 20 mL of HF (40 wt%) and stirred for 24 h to eliminate Al layer. After washing with deionized water until neutral, the black precipitate was dried to obtain multilayer Ti_3C_2.

Ti_3C_2/BiOBr composites was synthesized by the in-situ method. 2 mmol of $Bi(NO_3)_3 \cdot 5H_2O$ was added in 20 mL of a mixed acetic acid-water solution (volume ratio 1:20) with stirring for 10 min. Subsequently, a specified quantity of Ti_3C_2 powder was dispersed into the solution. 2 mmol of KBr was dissolved in 10 mL deionized water, and then mixed with the previous solution. Finally, the precipitate was obtained by centrifugation, washing and drying. The resulting products were designated as TB-x, where x = 10, 20, 50 were the mass ratio of BiOBr to Ti_3C_2. For comparison, BiOBr was synthesized using an identical procedure but without the inclusion of Ti_3C_2 powder.

2.2. Characterization

The crystalline phase was detected using X-ray diffraction (XRD, DX-2700B). Scanning electron microscope (SEM, Zeiss Gemini-300) was employed to observe the morphologic structure. Valence band (VB) and elemental states of the catalysts were measured by X-ray photoelectron spectroscopy (XPS, Thermoscience K-Alpha). Ultraviolet-visible diffuse reflectance spectra (UV-vis DRS) of materials were measured on a TU-1901 spectrometer.

2.3. Photocatalytic properties

The degradation of TC was conducted under simulated sunlight (500 W, 100 mW/cm^2). Briefly, 40 mg of prepared catalyst was added to tetracycline solution (100 mL, 20 mg/L) with stirring in the dark for 30 minutes. During this reaction, the absorbance of TC was detected by a UV-vis spectrometer.

To explore the active species during the degradation reaction, three scavengers were added to the photocatalytic system. Triethanolamine (TEOA, 15 mM), l-ascorbic acid (LAA, 1 mM) and tert-butanol (TBA, 10 mM) were used to trap h^+, $\cdot O_2^-$ and ·OH, respectively.

3. Results and discussion

The XRD patterns of Ti_3C_2, BiOBr, TB-10 and TB-50 are illustrated in Fig. 1. The diffraction peaks of Ti_3C_2 appear at $2\theta = 9.8°$, 18.3° and 60.6°, corresponding to the crystallographic planes (002), (004) and (110) [17, 18]. All peaks of prepared BiOBr sample are consistent with tetragonal phase BiOBr (JCPDS 09-0393) [19]. Due to the small amount of Ti_3C_2, the diffraction peaks of Ti_3C_2 cannot be seen in the XRD patterns of Ti_3C_2/BiOBr composites, indicating that the Ti_3C_2 Mxene has no effect on the crystalline phase of Ti_3C_2/BiOBr.

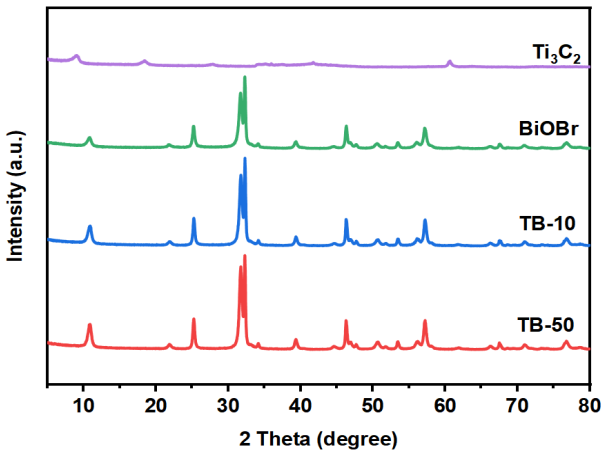

Fig. 1. XRD patterns of pure Ti_3C_2, BiOBr and hybrid catalysts.

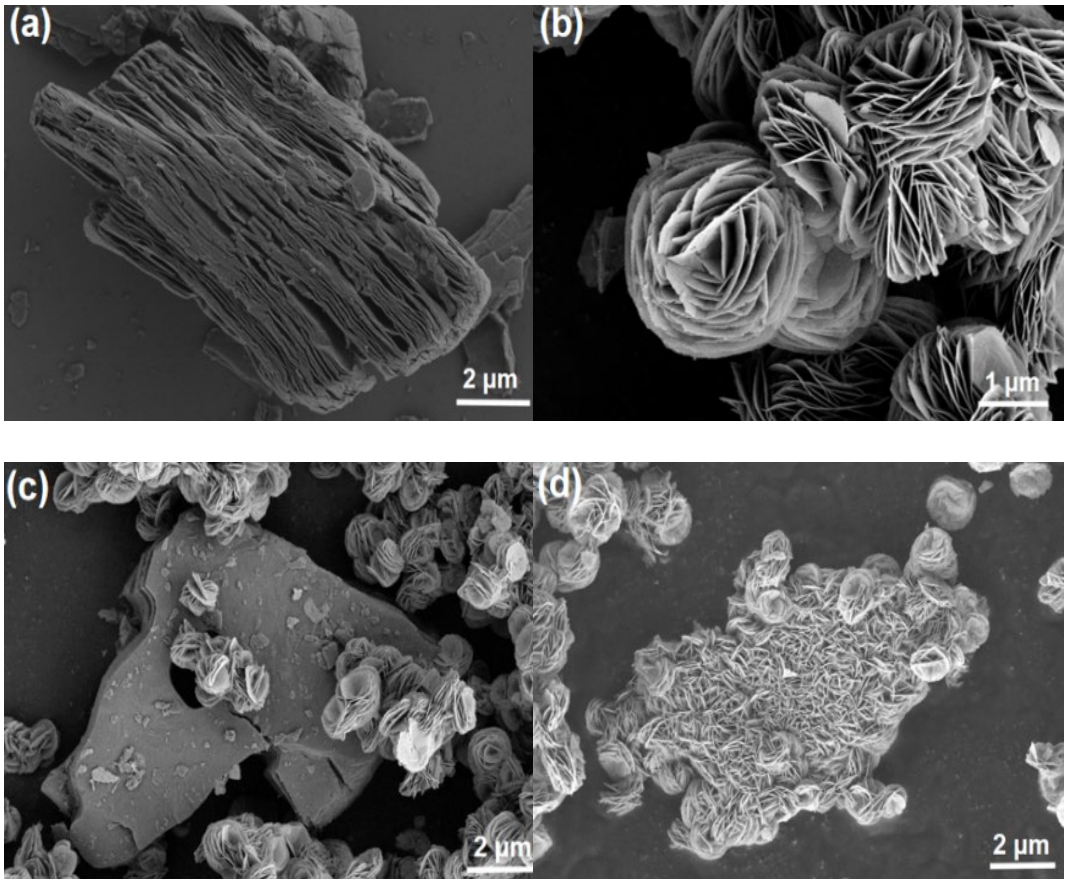

Fig. 2. SEM images: (a) Ti_3C_2, (b) BiOBr, (c) TB-10 and (d) TB-50.

Fig. 2 shows the morphology of Ti_3C_2, BiOBr and Ti_3C_2/BiOBr samples. It is found in Fig. 2a that Ti_3C_2 exhibits a typical layered structure composed of many nanosheets. As shown in Fig. 2b, BiOBr flowers are self-assembled from many nanosheets nanosheets, and the diameter is about

5 μm. For Ti_3C_2/BiOBr composites, it can be seen clearly that BiOBr microspheres are loaded on the surface and edge of Ti_3C_2 sheets (Fig. 2c). As the amount of BiOBr increased, more and more BiOBr flowers were grown uniformly on the surface of Ti_3C_2 (Fig. 2d), further confirming the successful coupling with of BiOBr.

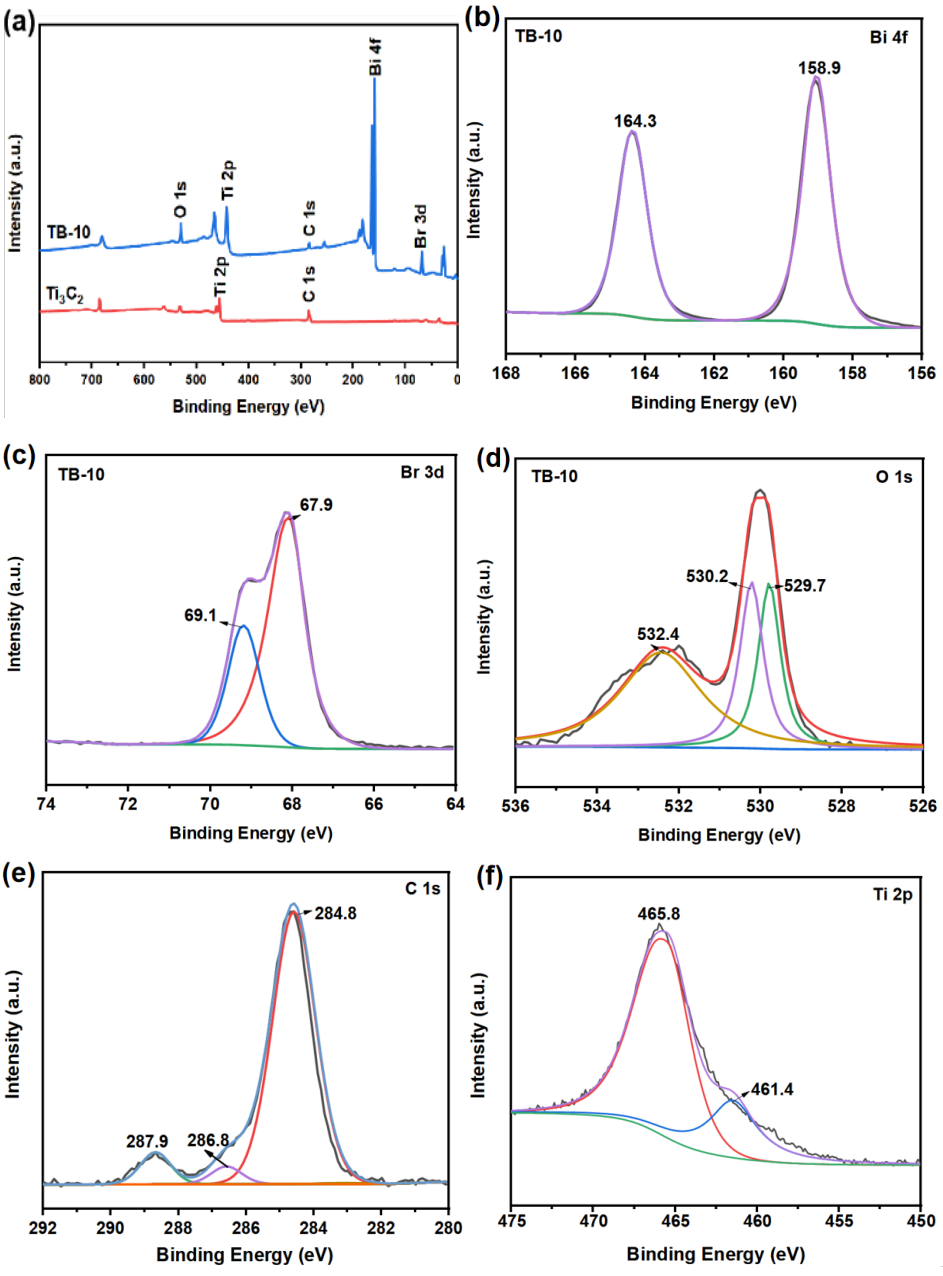

Fig. 3. XPS spectra of TB-10: (a) survey spectrum, (b) Bi 4f, (c) Br 3d, (d) O 1s, (e) C 1s and (f) Ti 2p.

The full XPS spectrum of the TB-10 catalyst is depicted in Fig. 3a and Br, Bi, C, Ti, and O elements are observed. The peaks of Bi 4f in Fig. 3b are 159.8 and 165.1 eV, belonging to Bi $4f_{7/2}$ and Bi $4f_{5/2}$, suggesting the presence of Bi^{3+} ions. Br 3d XPS spectrum (Fig. 3c) shows two peaks at 67.9 and 69.1 eV, matching with Br $3d_{5/2}$ and Br $3d_{3/2}$. As shown in Fig. 3d, three peaks at 529.7,

530.2 and 532.4 eV of O 1s are ascribed to O-Bi, Ti-O and O=C bonding groups, respectively [20, 21]. In Fig. 3e, the peaks at 284.8, 286.8 and 287.9 eV are indexed to C-C, C-O, and C-Ti bonds, respectively [22]. In Fig. 3f, two peaks at 461.4 and 465.8 eV are assigned to Ti $2p_{3/2}$ and Ti $2p_{1/2}$, respectively [23].

Fig. 4a displays the UV-vis DRS of BiOBr, TB-10, and TB-20. Compared with BiOBr, Ti_3C_2/BiOBr composites demonstrate stronger light absorption, which is beneficial for generating more photoelectron-hole pairs. The bandgap value (Eg) of BiOBr is calculated as 2.71 eV (Fig. 4b). XPS valence band of BiOBr is measured as 1.93 eV (Fig. 4c), and the VB calibration value of BiOBr can be evaluated as 2.09 eV by following equation [24]: $E_{NHE} = \varphi + E_{VL} - 4.44$. Additionally, the conduction band (CB) of BiOBr is estimate as -0.62 eV.

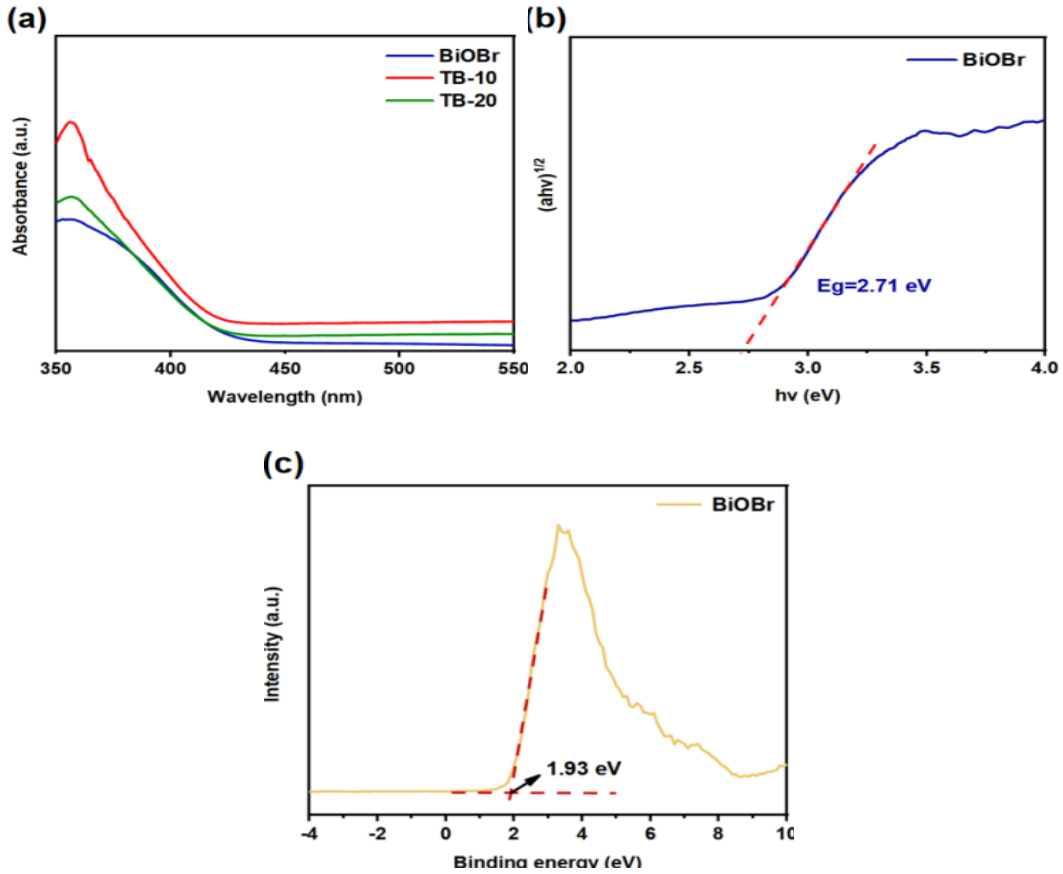

3Fig. 4. (a) UV-vis DRS of BiOBr, TB-10 and TB-20; (b) energy gap and (c) XPS valence band of BiOBr.

The photocatalytic performance of pristine Ti_3C_2, BiOBr, and Ti_3C_2/BiOBr composites are illustrated in Fig. 5a. After illumination of 30 min, 68.5% of TC has been degraded by BiOBr catalyst, while Ti_3C_2 has little effect on the degradation. In contrast, TB-x (x= 10, 20 and 50) hybrid catalyst show higher catalytic activity, and the degradation efficiency gradually improves with increasing BiOBr content. Obviously, TB-50 exhibits the highest degradation efficiency of 80.3%. The above

results indicate that Ti_3C_2 coupling with BiOBr could facilitate transfer of electron-holes, thus significantly boosting the removal efficiency of TC. Fig. 5b shows the pseudo-primary reaction rate constants for all materials. The kinetic constants (K) of the Ti_3C_2 and BiOBr catalysts are 0.00222 min^{-1} and 0.03803 min^{-1}, while TB-50 shows the largest rate of degradation with a constant of 0.04883 min^{-1}.

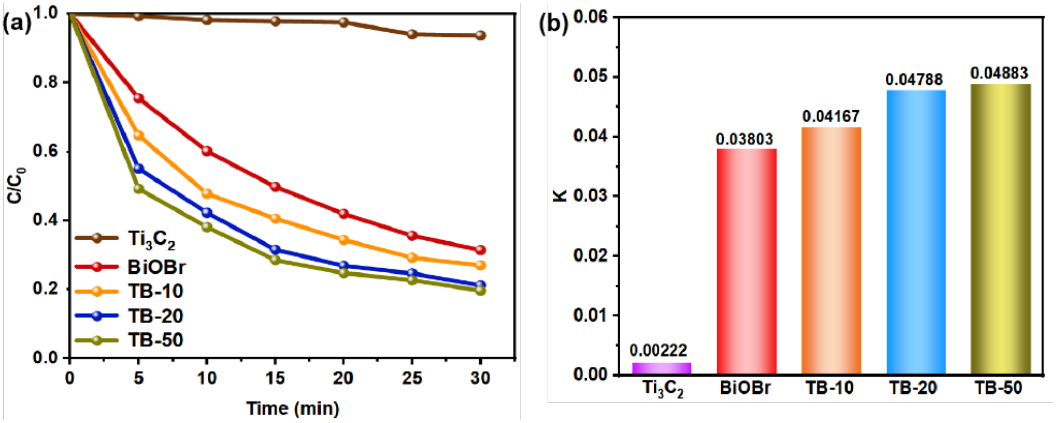

Fig. 5. (a) Photocatalytic decomposition of TC and (b) degradation rate constant.

Fig. 6a demonstrates the influence of three scavengers on the degradation efficiency with TB-50 sample. When TBA and TEOA were added, the degradation efficiency decreased to 74.5% and 64.3%, respectively. It is noticed that the removal efficiency greatly drops to 3.2% with the addition of LAA. This result reveals that $\cdot O_2^-$ is the predominant active species during TC degradation reaction.

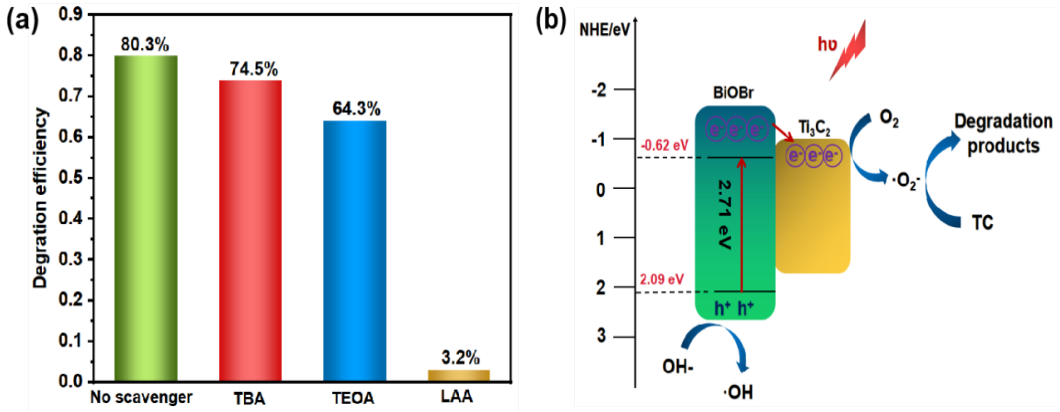

Fig. 6. (a) Trapping of active species; (b) photocatalysis mechanism of Ti_3C_2/BiOBr heterojunction.

The possible mechanism of Ti_3C_2/BiOBr heterojunction was proposed in Fig. 6b. Under irradiation, BiOBr generates electrons and holes, then the e^- in VB transfer to CB and h^+ accumulate in VB. Subsequently, a portion of the electrons on the CB of BiOBr can rapidly migrate into Ti_3C_2 and react with adsorbed O_2 to form $\cdot O_2^-$ with strong oxidizing ability. In this process, Ti_3C_2 with

good electrical conductivity functions as an electron trap that traps and stores photogenerated electrons, significantly facilitating carrier separation. Meanwhile, a portion of the h^+ can directly oxidize TC. Thus, the photocatalytic degradation of TC can be enhanced.

4. Conclusion

In summarize, layered structureTi_3C_2 were coupled with flower-like BiOBr microspheres by in-situ deposition method. Ti_3C_2/BiOBr composites showed stronger light absorption ability than pure BiOBr. The removal efficiency of TC improved gradually with increasing BiOBr content. When the mass ratio of Ti_3C_2 to BiOBr was 1:50, 80.3% of TC can be removed. The enhancement was ascribed to the Ti_3C_2/BiOBr heterojunction structure effectively promoting the migration of charge carriers.

References

[1] X. J. Du, J. Sun, Y. Li, W. H. Du, D. Jiang, Microchemical Journal 179, 107578 (2022); https://doi.org/10.1016/j.microc.2022.107578
[2] D. L. Cheng, H. H. Ngo, W. S. Guo, S. W. Chang, D. D. Nguyen, Y. W. Liu, Q. Wei, D. Wei, Journal of Hazardous Materials 386, 121682-121693 (2019); https://doi.org/10.1016/j.jhazmat.2019.121682
[3] S. H. Pu, Q. R. Zhao, X. Luo, D. Y. Q, K. Lei, Y. J. Duan, L. J. Mao, W. Feng, Y. Sun, Surfaces and Interfaces 46, 104016 (2024); https://doi.org/10.1016/j.surfin.2024.104016
[4] M. F. Li, Y. G. Liu, G. M. Zeng, N. Liu, S. B. Liu, Chemosphere 226, 360-380 (2019); https://doi.org/10.1016/j.chemosphere.2019.03.117
[5] Q. R. Zhao, S. Y. Chen, B. H. Ren, S. N. Liu, Y. C. Zhang, X. Luo, W. Feng, Y. Sun, Opt. Mater 135, 113266 (2023); https://doi.org/10.1016/j.optmat.2022.113266
[6] Y. Yang, D. Y. Wang, Y. C. Zhang, S. Y. Chen, Y. Sun, Dig. J. Nanomater. Bios. 17(4), 1491 (2022); https://doi.org/10.15251/DJNB.2022.174.1491
[7] J. Xu, W. Meng, Y. Zhang, L. Li, C. H. Guo, Applied Catalysis B: Environmental 107, 355-362 (2022); https://doi.org/10.1016/j.apcatb.2011.07.036
[8] Q. S. Huang, Y. T. Liu, T. Cai, X. N. Xia, Journal of Photochemistry & Photobiology A: Chemistry 375, 201-208 (2019); https://doi.org/10.1016/j.jphotochem.2019.02.026
[9] K. Liu, L. X. Wang, T. Fu, H. B. Zhang, C. M. Lu, Z. F. Tong, Y. Yang, Y. Peng, Chemical Engineering Journal 457, 141271 (2023); https://doi.org/10.1016/j.cej.2023.141271
[10] H. L. Zhang, M. Li, W. Wang, G. H. Zhang, Q. J. Tang, J. L. Cao, Separation and Purification Technology 272, 118911 (2021); https://doi.org/10.1016/j.seppur.2021.118911
[11] Y. Fang, Y. Cao, Q. L. Chen, Ceramics International 45, 22298–22307 (2019); https://doi.org/10.1016/j.ceramint.2019.07.256
[12] B. Sun, F. R. Tao, Z. X. Huang, W. Yan, Y. X. Zhang, X. H. Dong, Y. Wu, G. W. Zhou, Applied Surface Science 535, 147354 (2021); https://doi.org/10.1016/j.apsusc.2020.147354
[13] B. B. Fan, S. Y. Shang, B. Z. Dai, B. Zhao, N. Ling, M. Q. Li, L. J. Zhang, Ceramics International 46, 17085-17092 (2020);https://doi.org/10.1016/j.ceramint.2020.04.004

[14] J. Qu, D. G. Teng, X. M. Zhang, Q. Q. Yang, P. Li, Y. J. Cao, Ceramics International 48, 14451-14459 (2022); https://doi.org/10.1016/j.ceramint.2022.01.338
[15] Z. Q. Wang, Y. Y. Guo, Q. Zhang, Z. Y. Li, Y. Zhao, H. Y. Wang, Journal of Molecular Liquids 367, 120578 (2022); https://doi.org/10.1016/j.molliq.2022.120578
[16] X. Pang, S. X. Xue, T. Zhou, Q. L. Xu, W. Y. Lei, Ceramics International 48, 3659-3668 (2022); https://doi.org/10.1016/j.ceramint.2021.10.147
[17] S. S. Wu, Y. M. Su, Y. Zhu, Y. M. Zhang, M. S. Zhu, Applied Surface Science 520, 146339 (2020); https://doi.org/10.1016/j.apsusc.2020.146339
[18] J. H. Cai, A. X. Zhang, H. Tao, R. P. Li, J. H. Han, M. J. Huang, Physica E 145, 115476 (2023); https://doi.org/10.1016/j.physe.2022.115476
[19] L. F. Yang, J. Chen, M. D. Que, X. W. Liu, S. M. Zhu, Journal of Alloys and Compounds 893, 162289 (2022); https://doi.org/10.1016/j.jallcom.2021.162289
[20] Z. Z. Li, H. G. Zhang, L. Wang, J. J. Shi, Journal of Photochemistry & Photobiology A: Chemistry 386, 112099b(2020); https://doi.org/10.1016/j.jphotochem.2019.112099
[21] K. X. Gao, L. Hou, X. Q. An, D. D. Huang, Y. Yang, Applied Catalysis B: Environmental 323, 122150 (2023); https://doi.org/10.1016/j.apcatb.2022.122150
[22] T. X. Xu, J. P. Wang, Y. Cong, S. Jiang, Q. Zhang, H. Zhu, Y. J. Li, X. K. Li, Chinese Chemical Letters 31, 1022-1025 (2020); https://doi.org/10.1016/j.cclet.2019.11.038
[23] S. H. Huang, Y. Wang, J. Q. Wan, Z. C. Yan, Y. W. Ma, G. H. Zhang, S. L. Wang, Applied Catalysis B: Environmental 319, 121913 (2022); https://doi.org/10.1016/j.apcatb.2022.121913
[24] X. Q. Zhuang, Y. P. Huang, L. Q. Lin, W. T. Xu, X. B. Liu, Materials Letters 324, 132623 (2022); https://doi.org/10.1016/j.matlet.2022.132623
[25] T. Cai, L. L. Wang, Y. T. Liu, S. H. Zhang, W. Y. Dong, H. Chen, X. Y. Yi, Applied Catalysis B: Environmental 239, 545-554 (2018); https://doi.org/10.1016/j.apcatb.2018.08.053